Investigating the impact of impeller geometry for a stirred mill using the discrete element method: Effect of pin number and thickness

Osborne, T.; Rhymer, D.; Werner, D.; Ingram, A.; Windows-Yule, C.r.k.

DOI:
10.1016/j.powtec.2023.118810

Document Version
Publisher's PDF, also known as Version of record

Citation for published version (Harvard):
Osborne, T, Rhymer, D, Werner, D, Ingram, A & Windows-Yule, CRK 2023, 'Investigating the impact of impeller geometry for a stirred mill using the discrete element method: Effect of pin number and thickness', *Powder Technology*, vol. 428, 118810. https://doi.org/10.1016/j.powtec.2023.118810

Powder Technology 428 (2023) 118810

Contents lists available at ScienceDirect

Powder Technology

journal homepage: www.journals.elsevier.com/powder-technology

Investigating the impact of impeller geometry for a stirred mill using the discrete element method: Effect of pin number and thickness

T. Osborne, D. Rhymer *, D. Werner, A. Ingram, C.R.K. Windows-Yule

School of Chemical Engineering, University of Birmingham, Edgbaston, Birmingham, B15 2TT, UK

HIGHLIGHTS

- We vary attritor pin number with constant size and constant total projected area.
- Adding more pins of constant size strongly increases mean pair stress energy.
- Changing configuration of the same pin area has a much weaker effect.
- Pin spacing needs to be included when calculating the mill shear volume.

GRAPHICAL ABSTRACT

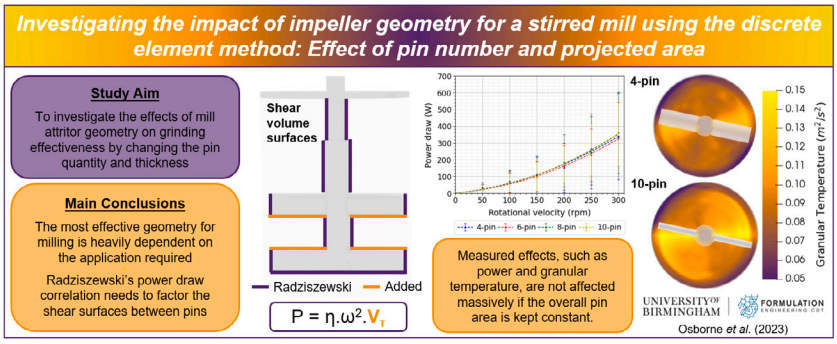

ARTICLE INFO

Keywords:
Vertical stirred mill
Discrete element method
DEM
Simulation
Milling
Attritor geometry

ABSTRACT

Vertical stirred milling is a major technique for grinding fine and ultra-fine particles. In this study, attritor designs of varying pin number and projected area were examined over a range of impeller rotational speeds using the Discrete Element Method (DEM). Analysis determined that additional pins improved the potential for effective grinding due to an increase of average collision energy. However, this was accompanied by a greater power draw. When projected area was maintained, there were fewer differences between designs, meaning that the specific configuration of the pins may not be as important. A template of the mill can be found at https://github.com/darhyme147/liggggghts_stirred_mill_template.

1. Introduction

Global demand for high-performance products containing fine particles is increasing, and grinding is vital to their production. Over 50% of products sold worldwide are powders or contain particulates, including sugars, cereal, sand and cocoa [1]. However, as a unit operation, grinding and comminution contributes one of the highest energy consumption rates; the mining sector alone was responsible for an estimated 1.8% of global electrical energy consumption in 2015 [2]. Moreover, efficiency values can be as poor as 1%–2% [3], so reducing energy use while maximising grinding quality is of paramount interest to industry, especially considering the current global economic and energy climate.

Stirred media milling is extensively applied as a grinding technique, since its relatively high impact energies provide greater size reduction efficiency and lower energy consumption in comparison to horizontal ball milling [4,5]. Several forms of stirred mills exist with each having favourable characteristics for use in certain industries. The first example was a "stirred ball mill" prototype developed by Klein and Szegvari in 1928 [6]. In 1946, this evolved into the modern-day "Attritor mill", a vertically operated pin mill that could grind particles even at low tip speeds. Since then, several variations have

* Corresponding author.
E-mail address: dcr502@bham.ac.uk (D. Rhymer).

https://doi.org/10.1016/j.powtec.2023.118810
Received 7 February 2023; Received in revised form 7 July 2023; Accepted 11 July 2023
Available online 17 July 2023

been manufactured using this design template [7]. Generally, vertical designs are used in industry due to their relatively high energy density and low physical footprint [8].

Experimental and theoretical investigations have improved understanding of grinding mechanisms and performance of stirred mills. A mechanistic stress model was developed by Kwade et al. [6,9], which transformed a specific energy input into a grinding bead stress intensity, a metric that can be optimised to produce the finest ground product. This is stated as

$$SI \propto SI_M = d^3 \cdot \rho \cdot (v_{ij}^t)^2, \tag{1}$$

with SI_M being the stress intensity of the media; and is a function of its diameter, d, density, ρ, and tangential velocity, v_{ij}^t. Over time this model was adapted and its accuracy improved. Breitung-Faes and Kwade [10] introduced geometric and material parameters to enhance the original model. Here the dominant stress mechanism was assumed to be compression, expressed by material parameters of compression strength and Young's modulus. Energy transfer coefficients were also introduced to enable calculation of specific power input for particular grinding outcomes. Radziszewski et al. [11] used dimensional analysis of a stress intensity relationship to form a characteristic physical parameter for stirred mill geometries and predict mill power. Tokoro et al. [12] dissociated collision events and developed a relationship between grinding performance with respect to kinetics, power consumption, and limiting particle diameter. However, little research has focused on the impact of impeller geometry on flow properties and the grinding performance of stirred mills.

In the context of optimising the geometry of an impeller, the Discrete Element Method (DEM) is a valuable modelling technique which provides insight that would otherwise be experimentally demanding. The development of parallel and multi-core computing since the early 2000's has enabled researchers to simulate progressively larger granular systems with a widening variety of applications, including: mills [13–15], granulators [16], mixers [17], hoppers [18] and drums [19]. Although the application of DEM to milling still has computational limitations, over 10^6 particles may now be simulated in a reasonable timescale (within one week). Useful information describing collision kinetics and grinding media dynamics can be extracted to predict the effectiveness of a stirred mill. Blais et al. [1] recently considered the method and numerical implementation of DEM, scrutinising and reviewing a range of applications. The article concluded that DEM is an accurate and versatile tool, highlighting its ability to model granular flows and potential to extend into multiphysics applications, along with coupling to CFD to describe solid–liquid systems. Important challenges were also identified, such as the calibration of parameters including sliding and rolling friction, damping coefficients and the coefficient of restitution, which all depend on powder and flow profiles [20,21].

The central impeller has a large potential for geometrical variation, with configurations in industry including disc [22], pin, screw (tower) [23] and combinations of these [11]. Thus, optimising the geometry could have a vast impact on the energy-effectiveness. Impeller design and operating conditions have been determined empirically in industrial procedures, but with the adoption of simulation methods, wider reaching and more systematic investigations have been possible. A comparative study by Plochberger et al. [24] showed that a mill had better energy transfer, greater power intensity and absorbed more input power if designed with a pin impeller compared to a disc impeller. A separate DEM based study by Cleary et al. [8,25] of a 1.5 kW tower mill and a 7.5 kW pin mill showed the tower mill had more favourable comminution properties. It was shown to be capable of both convective axial and diffusive radial mixing (the pin mill displayed poor axial mixing), and the superior particle transport led to a larger proportion of particles reaching high breakage areas. Therefore the tower mill possessed better grinding capabilities despite the pin mill having greater levels of energy absorption. Eswaraiah et al. [26] had previously made the same conclusions experimentally.

Due to difficulty in isolating variables and the financial constraints of developing multiple physical designs, the extent of research of impeller designs has been limited and often only looks at a handful of designs [6]. A study that specifically targeted the impact of impeller geometry in a vertical stirred pin mill was done by Daraio et al. [14], who investigated the effect of arm length on grinding media motion. The authors concluded that a longer arm was more effective in promoting media agitation as the size of regions of maximum shear decreased. Tokoro et al. [12] compared the performance of three different pin impeller designs with varying directions relative to the shaft. The best results were when the pins were perpendicular, as it produced the narrowest particle distribution, and thus faster and finer grinding. However, the study was conducted in the horizontal orientation. The impact of varying pin number and size has not been included in literature.

In the present work, impeller pin number was varied under two constraints: constant size for each pin, and constant projected surface area for all pins. DEM simulation provided a detailed description of the grinding media interactions for each tested geometry, with the base model having been created and validated in a previous work [15]. The rotational speed of the impeller was varied to investigate the influence in different regimes. The interaction of 10 mm grinding media was modelled with an assumption that no media wear occurred over the simulation time frame investigated. In physical systems, the particulates needing to be ground are significantly smaller than the grinding media, so these are incorporated into the media restitution and friction values. This study aimed to extract system kinetics and analyse granular flow properties to identify an impeller design that provides maximal grinding effectiveness while limiting energy waste.

2. Methodology

2.1. Discrete element method

The open source DEM software LIGGGHTS® (LIGGGHTS v3.8.0, DCS Computing GmbH, Austria) [27] was used to model grinding media interactions. Simulations track translational and rotational particle motion in granular systems by applying Newton's second law [15,28]. The resultant forces of two particles in contact can be see in Fig. 1, and from this, equations describing the normal and tangential forces are defined.

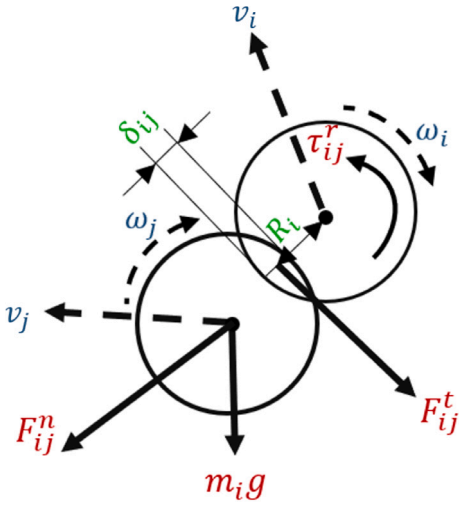

Fig. 1. The resultant velocities (blue) and forces (red) of two particles, i and j, in contact with each other [14].

$$m_i \frac{dv_i}{dt} = (F_{ij}^n + F_{ij}^t) + m_i g, \tag{2}$$

$$I_i \frac{d\omega_i}{dt} = (R_i \times F_{ij}^t - \tau_{ij}^r). \quad (3)$$

m_i, I_i, v_i, ω_i represent the mass, moment of inertia, translational velocity and rotational velocity respectively. τ_{ij}^r is the rolling friction torque, R_i is the radius, and $m_i g$ represents the particle weight. F_{ij}^n and F_{ij}^t are the normal and tangential forces acting on the particles, are calculated according to a non-cohesive Hertz–Mindlin no-slip contact model [14];

$$F_{ij}^n + F_{ij}^t = (K^n \delta_{ij}^n - \gamma_n v_{ij}^n) + (K^t \delta_{ij}^t - \gamma_t v_{ij}^t), \quad (4)$$

where $(K^n \delta_{ij}^n - \gamma_n v_{ij}^n)$ and $(K^t \delta_{ij}^t - \gamma_t v_{ij}^t)$ are the normal and tangential forces. Both expressions are quantified as the difference between a spring and damping component. Each of the spring components contain a stiffness component which is calculated using effective values for radius, R^*, Young's modulus, E^*, shear modulus, G^* and contact overlap, δ_{ij},

$$K^n = \frac{4}{3} E^* \sqrt{R^* \delta_{ij}^n}, \quad (5)$$

$$K^t = 8 G^* \sqrt{R^* \delta_{ij}^n}. \quad (6)$$

The Hertz–Mindlin model is the most common in DEM simulation due to its accuracy, simplicity, and robustness [29], although it excludes attractive surface energy forces, such as van der Waals interactions. For the current study, which models large, heavy particles, this is a reasonable assumption as any attractive (cohesive) forces are expected to be sufficiently small compared to the media contact forces.

2.2. Computational model & validation

The base model is the same one as used in the previous study: *"A discrete element method investigation within vertical stirred milling: Changing the grinding media restitution and sliding friction coefficients"* [15]. In this work, the model had been validated and calibrated from previous work by Daraio et al. [14,30], who validated a dry powder vertical mill using Positron Emission Particle Tracking (PEPT) data and then used the resulting model in their pin length study previously mentioned. This meant that there was no requirement for coupling with any fluid methods, like Computational Fluid Dynamics (CFD). In the interests of open and transparent science, a sample copy of the template mill can also be found at https://github.com/darhyme147/liggggghts_stirred_mill_template, so scientists and researchers are able to use this template for their own work or reproduce the findings of the paper in more detail.

Table 1
The material input parameters used for each simulation.

Parameter	Value
Media diameter, d (mm)	10.0
Media density, ρ (kg m^{-3})	7850
Young's Modulus (N m^{-2})	2.1×10^7
Poisson ratio, ν (–)	0.3
Restitution coefficient, ε (–)	0.7
Sliding friction coefficient, μ_s (–)	0.25
Rolling friction coefficient, μ_r (–)	0.0
Media fill level (%)	55
Time step, t (s)	10^{-6}

The material properties are given in Table 1. These were taken directly from the previous work and are based on the physical properties of stainless steel. The effect of rolling friction can be ignored when the motion of spherical grinding media is considered [8,25]. The value for the coefficient of restitution, 0.7, was extracted from the investigations of collisions completed by Radil and Palazzolo [31]. This is towards the upper limit of the real value range which would be observed, but still provides a reasonable estimate for the results, particularly on a qualitative basis. Data was recorded for ten seconds in total, after the mill had been allowed to stabilise at a steady state. The mill was filled to 55% of the available volume which follows on from previous work [14,15]. This equated to 4379 media beads.

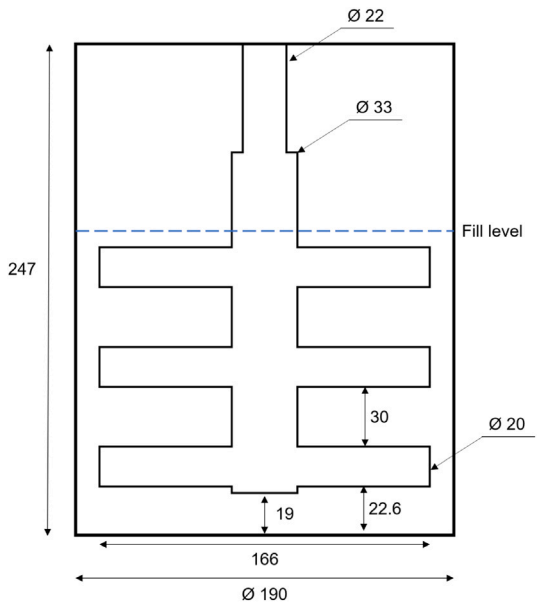

Fig. 2. Figure showing the dimensions of the 6-pin geometry used in the constant pin size investigation. All dimensions are in mm.

2.3. Mill geometry

Fig. 2 illustrates a 2D schematic of the 6-pin impeller used in the constant pin size study. The outer vessel, attritor shaft diameter, pin length and pin diameter (within the constant pin size investigation), are based directly off previous work [14,15].

Adding pins to the central impeller shaft appears logical for better grinding as it increases the surface area for interaction between grinding media and the impeller. However, this action could also lead to changes in the flow of media, since a varying pin distribution and separation changes flow properties and media interactions. Isolating the impact of increasing surface area by keeping the total projected surface area of all pins constant is necessary to dissociate the influence of surface area and other impeller features. Accordingly, the investigation was formed of two parts. The first was to simply change the number of pins on the shaft, while the second maintained the total projected surface area of all pins. Each study varied the number of pins between four and ten. A fixed pin length of 83 mm was used to maintain a constant tip speed at the same rpm values. Each attritor geometry is shown in Fig. 3 and Appendix lists the key attritor dimensions.

2.4. Post-processing

One of the biggest advantages of simulation is that no experiment is able to generate the same volume and quality of data in a comparable timescale [32]. This can be further post-processed to add context and meaning.

2.4.1. Granular temperature

Grinding is only possible if the media are interacting with each other in a disruptive manner and therefore, a useful method to illustrate grinding effectiveness of the media is to measure velocity fluctuations relative to a local mean. This metric is known as the granular temperature and is given as

$$v_G = \frac{\sum v_{cell}^2}{n_{cell}} - \bar{v}_{cell}^2, \quad (7)$$

where v_G is the granular temperature and v_{cell} is the velocity of the media within each cell. Granular temperature is similar to thermal

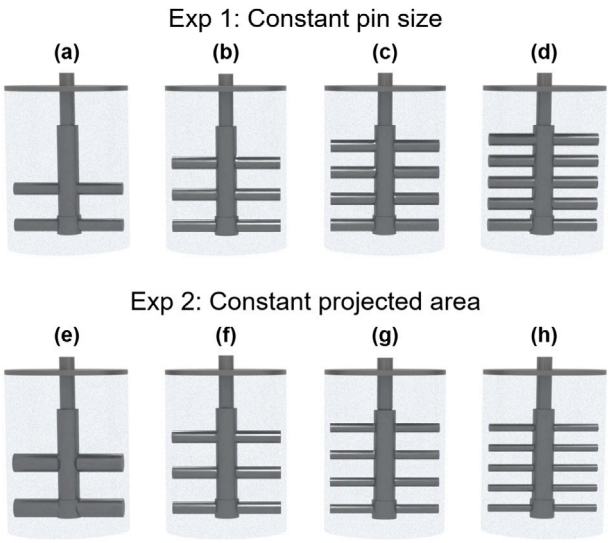

Fig. 3. Figure showing the different geometry designs used in the constant pin size: (a) 4-pin, (b) 6-pin, (c) 8-pin, (d) 10-pin, and constant projected area: (e) 4-pin, (f) 6-pin, (g) 8-pin, (h) 10-pin simulations.

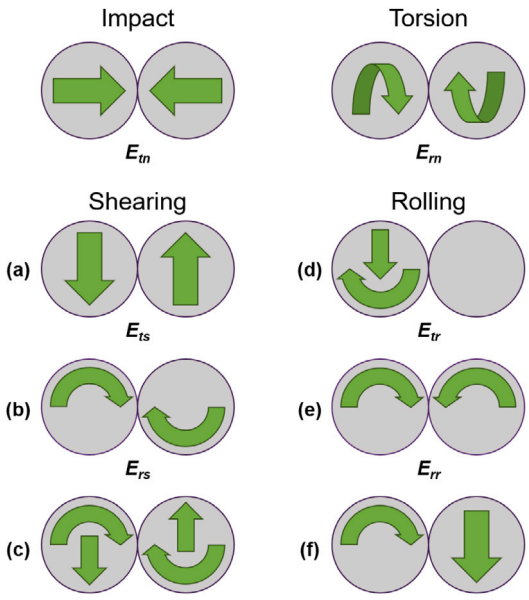

Fig. 4. The eight collision mechanisms presented by Beinert et al. [34], separated into impact, torsion, shearing and rolling effects [15].

temperature in the kinetic theory of gases. A low value indicates possible solid body motion as media are not moving with respect to one another; a phenomenon which hinders grinding [33]. Although time averaged when presented, a reference frame was taken with respect to the pin motion, meaning that the cells rotated in line with the system, and therefore, the same relative space could be analysed consistently, even with respect to time.

2.4.2. Collision energies

Computational modelling has allowed researchers to gain an in depth understanding of milling at collision level. As no physical grinding takes place in most simulations due to processing limitations, the effectiveness is assumed as a probability for a particle to be milled if it was to be included. The most common metric to identify this is by looking at the energy spectra that are produced from the collisions in the simulation. Beinert et al. [34] studied this principle and determined that a pair of spherical beads in contact would exhibit at least one of six main collision mechanisms, shown diagrammatically in Fig. 4 [15].

Table 2 shows the associated Equations for the different collision energies that can be derived from each of these mechanisms. A more detailed explanation of each can be found in Rhymer et al. [15]. The total energy of collision, E_{total}, is the sum of all six components. In literature, abrasion has been most frequently identified as the dominant breakage mechanism in stirred mills, especially for fine grinding in the low impeller speed range [35–37].

Table 2
The six Equations defining contact pair collision mechanisms [34].

Mechanism	Symbol	Equation	
Impact	E_{tn}	$E_{tn} = \frac{1}{2} m (v_{ij}^{n})^2$	(11)
Torsion	E_{rn}	$E_{rn} = \frac{1}{5} m r^2 (\omega_{ij}^{n})^2$	(12)
Shearing	E_{ts}	$E_{ts} = \frac{1}{2} m (v_{ij}^{t})^2$	(13)
	E_{rs}	$E_{rs} = \frac{1}{5} m r^2 (\omega_{ij}^{t})^2$	(14)
Rolling	E_{tr}	$E_{tr} = \frac{1}{2} m (\boldsymbol{v}_i + \boldsymbol{v}_j)^2$	(15)
	E_{rr}	$E_{rr} = \frac{1}{5} m r^2 (\boldsymbol{\omega}_i + \boldsymbol{\omega}_j)^2$	(16)

2.4.3. Power draw

Power is a highly important grinding metric because it indicates how efficient a mill is. It is also one of the few outputs which researchers are able to obtain in both simulation and experiments, allowing for direct comparison between the two. While there is no direct output in LIGGGHTS, the normal media-media power draw, P, was sampled for each time output by summing the product of the dissipative force components from Eq. (8), F_{diss}, and relative velocity, v_{rel}, for each contact,

$$P = \sum_{i=1}^{n} F_{diss}(i)\ v_{rel}(i). \tag{8}$$

Normally, Eq. (8) is, in fact, the integrated velocity over the course of the contact. However, in our case, all contacts are simultaneously sampled at a fixed time point such that instantaneous velocity is constant and the system state is steady enough to assume that power is similar at any sample point since we are averaging collisions at each stage of contact. There are two ways of obtaining the dissipative force in LIGGGHTS from the Hertz–Mindlin derivation (see Eqs. (4)). Either by calculating γ_n or γ_t directly, or through solving the force balance from the normal and tangential force outputs that LIGGGHTS gives. The latter was used because it is calculated from outputs rather than inputs so absorbs any simulation errors, such as in rounding.

Several papers have investigated the derivation of more universal power draw formulae, with Herbst and Sepulveda [38] deriving an equation using multiple regression of data points for stirred media mills that incorporated rotational speed, mill volume, media diameter and media density. Kwade et al. [39] derived a now well-established stress model which Radziszewski and Allen [11,40] later used to derive a power draw model based on a fluid mechanics definition of shear stress and an assumption that the main breakage mechanism is abrasion. The pair concluded that power followed a quadratic proportionality with impeller rotational speed, ω, with the function producing a relatively good fit when plotted versus experimental data for three varieties of stirred mills:

$$P = \eta \omega^2 V_{\tau}. \tag{9}$$

η is the dynamic viscosity of fluid in the system. It is estimated from correlations by Gao, Forssberg and Weller [41]. V_{τ} is "shear

volume" [11,40],

$$V_\tau = A\frac{r_s^2}{y}, \tag{10}$$

where A is the total area undergoing shear, r is the radius over which the shear is acting, and y is the separation of shear surfaces. Appendix shows the calculated values for V_τ in each instance using Radziszewski's original definition. These are the summation of the V_τ values for the pin tips, the shaft and the bottom pin surface. Dynamic viscosity is assumed to be constant for all scenarios.

3. Results and discussion

3.1. Velocity & granular temperature

The simplest measure of milling potential is velocity as it is proportional to the kinetic energy present. Fig. 5 illustrates a monotonic trend of average media velocity with attritor speed for all simulations. The trend is slightly non-linear, with the gradient progressively decreasing. This is a result of greater power dissipation per collision and reduced contact of beads from increased fluidisation (See Section 3.4). The total contact area between pins and media is more important than the way it is configured, with the total projected area simulations, (b), showing a much tighter distribution of media velocities at the same attritor rotational speed. At low speeds, this is even smaller because the lack of energy driving the media upwards means the 4-pin designs, with lower centre of mass, are a lot more comparable. At higher attritor speeds, the media velocity favours the 10-pin design a little more because the area is distributed more evenly throughout the milling height.

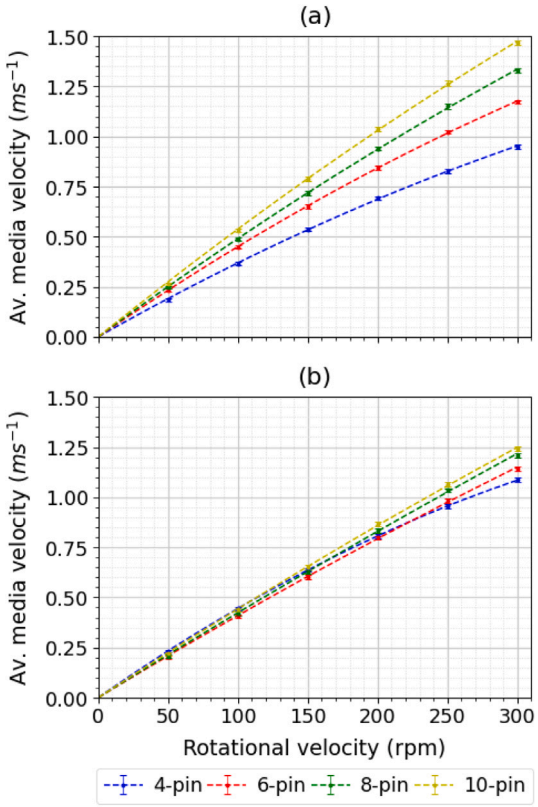

Fig. 5. Average media velocity as a function of impeller rotational speed for each impeller design. (a) constant pin size and (b) constant projected area. Lines are to aid the reader's interpretation.

Fig. 6 shows the flow fields of each design at 300 rpm. For both experimental sets, a high energy region can be observed around the pin tips, with this becoming larger and more intense as the number of pins increases. There is an overarching recirculatory motion observed in all cases where the media push out and upwards at the vessel walls until they reach the top of the milling space and cascade back down. However, there are individual recirculation loops present in some of the designs, particularly when the number of pins are low, creating more gaps for media to flow between. When higher numbers of pins are used, the increased steric hindrance creates a wall that the media struggle to pass through. There is a much lower velocity region below the bottom layer of pins in all cases. This decreases in size when the individual pins are larger, as shown in (e), because there is a greater amount of momentum from the pins. Industrially, this is quite important because there have to be clearances between attritor and vessel to prevent jamming, often making the bottom region very low energy. If larger pins are used in that region, they would be able to induce a greater amount of motion within the media without breaking any engineering tolerances that need to be considered.

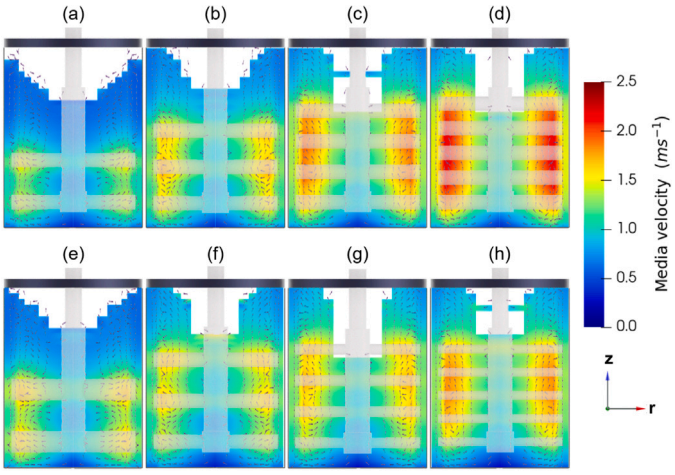

Fig. 6. Velocity fields of all designs in the r-z plane at 300 rpm with arrow lines marking direction of flow. Constant pin size: (a) 4-pin, (b) 6-pin, (c) 8-pin, (d) 10-pin. Constant projected area: (e) 4-pin, (f) 6-pin, (g) 8-pin, (h) 10-pin.

The granular temperature is observed to increase with impeller speed (Fig. 7). This is a result that is expected to correlate to collision frequency, implying that higher impeller speeds cause more collisions and thus more opportunity for momentum transfer. Moreover, a higher impeller speed imparts more momentum transfer per collision, further contributing to increasing the velocity of the media. Higher impact velocities at higher impeller speeds are evident from the monotonic trend of granular temperature and impeller speed, illustrating that greater variance in velocity is present in the high impeller speed regime. Outgoing velocities are thus reduced, limiting the average system velocity. Hence, the gradient of the average velocity curve shown in Fig. 5 is slightly non-linear with attritor speed. For a constant pin size, impellers with greater numbers of pins generated a higher mean particle velocity because the total projected surface area increased with each additional pin, forming a larger area for collisions and momentum transfer between pins and particles. Putting this into depth-averaged surfaces (Fig. 8) shows that the highest fluctuations occur closest to the pins tips as this is where the highest input energy is. In all cases, there is a gradual decrease in V_G as the circular distance from the pin increases. Where the projected area is greatest (Fig. 8(b)), the granular temperature is highest and most consistent through the mill. Apart from at the tip, where number of pins produces a higher V_G due to a larger distribution of energy across the mill height, there is a more consistent granular temperature when projected energy is fixed, (c) and (d), compared to when pin number is increasing, (a) and (b).

3.2. Force

To better grasp the grinding mechanisms involved, the average force transferred to the media was evaluated. It is a useful metric for

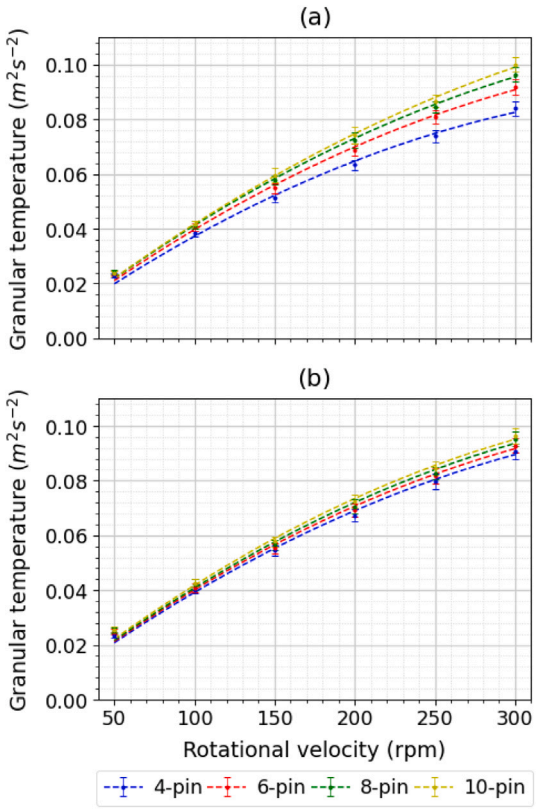

Fig. 7. Granular temperature versus impeller speed for (a) constant pin size and (b) constant projected area.

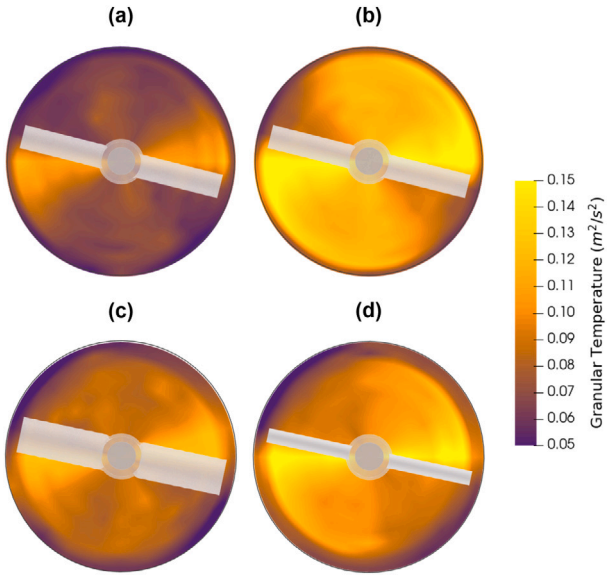

Fig. 8. Depth averaged $r-\theta$ granular temperature plots of the mill with constant pin size: (a) 4-pin, (b) 10-pin, and constant projected area: (c) 4-pin, (d) 10-pin. All mills are rotating anti-clockwise at 300 rpm and the frame of reference is set to the attritor.

measuring grinding effectiveness, since greater collision force improves the chances of breakage by impact. Fig. 9 illustrates the relationship between average media force and impeller speed, which like the velocity plot in Fig. 5, showed a monotonic trend. Furthermore, as pin number increased, the force transferred to the media increased, with the distribution narrowing when area was kept constant due to a constant interaction area for force transfer. A higher population of pins was concluded to form a more turbulent flow regime in the system, thus increasing force transfer in collisions. This was justified by a non-linear positive correlation between pin number and granular temperature as more significant velocity fluctuations provided an indication of chaos in the system. The importance of this industrially is if a greater number of pins cause more chaos, it increases the chance of the media coming together with enough force to have successful collisions and increase grinding.

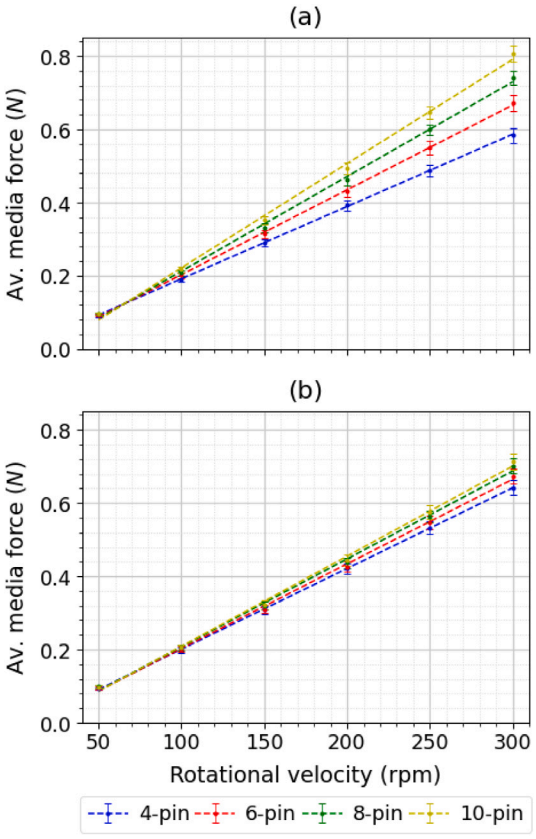

Fig. 9. Average media force versus impeller rotational speed for each impeller design for (a) constant pin size and (b) constant total pin projected surface area.

3.3. Contact energies

The energy spectra of the media are provided in Fig. 10. Fig. 10(d) shows minimal difference in the energy spectra when the projected area is kept constant and the velocity is high enough to reach all pins, suggesting that configuration is largely insignificant. This is because in fixing the area, the amount of input energy being supplied is roughly equal, providing that the media are able to create enough lift that they reach all pins. There are slightly higher energies with increased pin number but these are not as large as some of the other observations presented. Industrially, this could be highly significant, as attritors can therefore be designed with the knowledge of maximising the projected area, but with fatter, more durable pins. While similar energy spectra is the case at 300 rpm, it is not at 50 rpm (Fig. 10(c)). Here, the 4-pin has a higher intensity spectrum because more of the pin area is sat within the media. There is insufficient media volume and energy input to utilise the top pins within the design, so they are not able to transfer any of their rotational energy.

When the individual pin area is kept the same and the number of pins are increased, as in Fig. 10(a) and (b), the spectra show that a greater number of pins increases the amount of energy present. This is expected as more energy is being supplied. At 50 rpm, there is a change between the four and six pin simulation but less of an additional

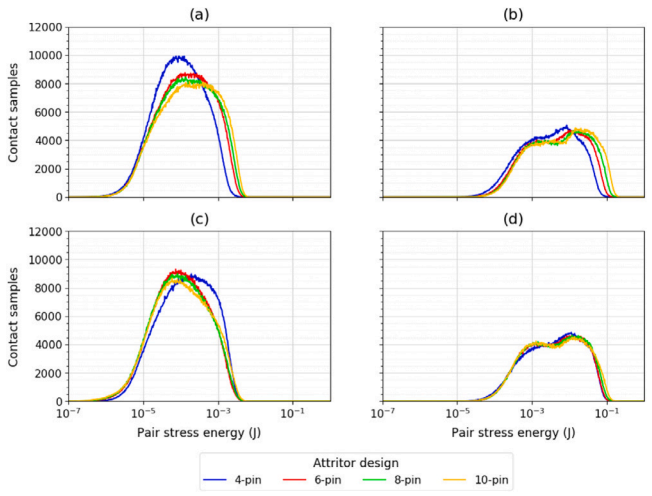

Fig. 10. Logarithmic collision energy spectra with constant pin size: (a) 50 rpm, (b) 300 rpm, and constant projected area: (c) 50 rpm, (d) 300 rpm.

effect as further pins are added because again, they start to sit above the media. This is less of an issue at 300 rpm, as there is enough lift created for the media to fill the mill, so all of the available pins are contributing towards successful milling performance. This means that an optimal design for collision energies would have as much projected surface area as possible for milling, yet still allow for the media to move and interact throughout the entire active region.

3.4. Power draw

Fig. 11 illustrates the overall power dissipation in both studies. At low impeller speeds the grinding media settle, forming an inhomogeneous occupancy within the mill, whereas at high impeller speeds, the media are concentrated towards the system walls due to the centrifugal force they experience. Consequently, the relationship between power draw and impeller speed can vary considerably, especially as the data is sampled. Additionally the flow properties of the media are dependent on other factors such as material loading and media density, hence theoretically analysing mill power is complex. Therefore, empirical formulae are generally valid solely for the particular system they are applied to. A quadratic curve gave an acceptable fit for each design with respect to rotational velocity. The constant pin size set, (a), showed that power draw increased as pins were added. This was because more obstacles were present and thus, greater turbulence. The presence of turbulent flow and the level of shear in the system are coincidental [42], with velocity fluctuation describing the chaotic characteristics of a system that contribute to both phenomena. The constant area results, (b), give more interesting results because, like with velocity, the distribution between designs at the same attritor speed are very tight, and often do not follow in order of the number of pins present. This is because of the different surfaces in contact with the media. At low rpm, the 4-pin design is more submersed within the media so all of the attritor volume is interacting, whereas some of the designs with higher pin numbers do not have this.

The derivation by Radziszewski, Eq. (9) [40], was applied and the corresponding shear volumes are in Appendix. As pin number increases while size is kept constant, the shear volume increases. It was assumed that dynamic viscosity is constant across all cases. The power draw presented in Fig. 11(a) correlates to this, with the higher number of pins exerting more power, although with a larger ratio that Radziszewski's prediction. However, there is an opposite effect in Fig. 11(b) as the 4-pin design, which has the biggest calculated shear volume, dissipates the lowest power at high velocities. As Radziszewski only investigated

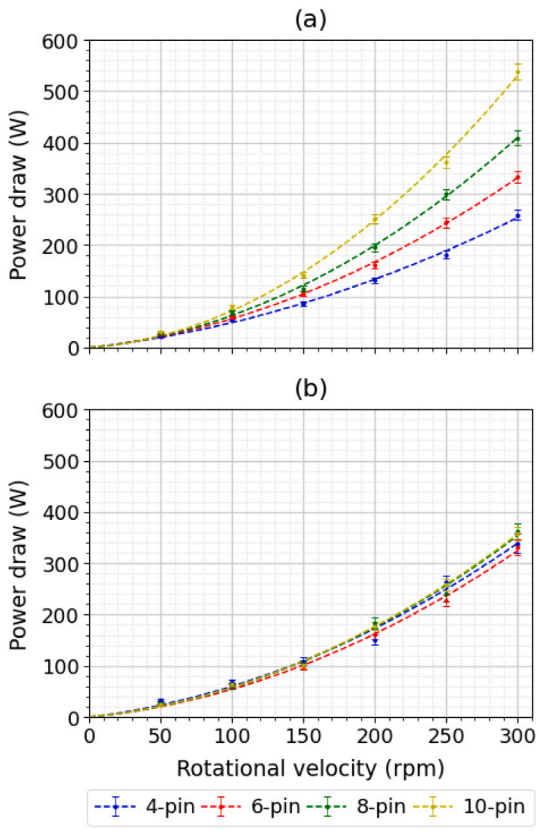

Fig. 11. Average power draw versus impeller rotational speed for each impeller design. (a) constant pin size and (b) constant projected area.

the power between different types of mill with similar dimensions, and not different configurations of the same type, there could be parameters needed in addition to his design equation, such as number of pins, placement and spacing. When comparing across the two experiments, the power draw trend is coherent with the shear volume trends. The 4-pin, which has greater V_τ in the constant area set, has a greater power draw in Fig. 11(b). Likewise, the 8-pin and 10-pin designs have a greater V_τ in the constant pin size study, and draw a greater power in Fig. 11(a). The 6-pin, which has a nearly identical V_τ in both experiments, shows very similar results in both cases.

Radziszewski concluded that his shear volume was deemed to have needed further analysis to be used with confidence [11]. If the derivation is now applied, but the previous shear volume is calculated with the addition of the shear surfaces between the pins, as shown in Fig. 12 and Table 3, the correlations become more aligned because the new shear volume favours the greater number of pins if the whole attritor is actively shearing. This makes sense because even though adjacent pins have the same speed, there is a velocity gradient to the fluid and beads in between. Rotational velocity will have an effect on these additional shear surfaces due to the vortex created by the mill. This means some surfaces will not have full contact with the media, reducing the shear volume. Likewise, low velocity mills may not contain enough energy to reach all shear surfaces. Overall, the modified equation shows qualitative agreement in most cases, with further research required to validate the theory across a greater range of cases.

In both studies but particularly while the surface area was constant, there is an overlap at low rotational speeds. Studies in which impeller rotation rate has been varied have agreed with these observations. In particular, Daraio et al. [14] found a monotonic trend between power dissipation and rotation speed with differences in power dissipation between designs negligible at low speeds. This overlap also comes from variance due to the instantaneous nature of the sampling rate.

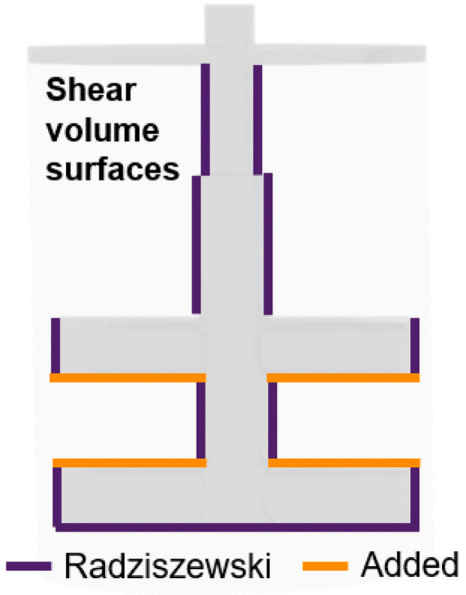

Fig. 12. Indicated shear surfaces which are used to form Radziszewski's shear volume [11], and the additional surfaces, considering the separation between pins, which have been proposed.

Table 3
Calculated shear volume of each design using the Radziszewski definition without accounting for pin spacing, V_τ and the inclusion of a shear surface between adjacent pins, $V_\tau(new)$.

		4-pin	6-pin	8-pin	10-pin
Const pin size	V_τ	0.0010	0.0014	0.0017	0.0021
	$V_\tau(new)$	0.0018	0.0031	0.0053	0.0096
Const pin area	V_τ	0.0021	0.0014	0.0011	0.0009
	$V_\tau(new)$	0.0031	0.0029	0.0032	0.0040

3.5. Effectiveness of power transfer

In industry, there normally has to be a compromise between effectiveness and efficiency and this needs to be considered. The study was extended to two investigations of power transfer effectiveness: a comparison of force transfer and power dissipation and a comparison of particle rotational rate and that of the impeller. To gain an understanding of the efficiency of force transfer to grinding media in the system, a metric of average force acting on grinding media per unit of power dissipated was evaluated; its relationship with impeller speed is illustrated in Fig. 13. Adding pins of constant surface area produced a negative correlation between this quantity and speed of the impeller, with a negative linear correlation deemed an appropriate fit. Since force exhibits a linear trend with impeller speed, while power displays a quadratic one (especially in the higher speed regime), a reciprocal relationship between a force-power draw ratio and impeller speed was expected. However, it was deduced that the data set was insufficiently large to display this. Systems containing fewer pins consistently displayed more effective force transfer to media. This result was expected since force transferred had little variance between designs, especially for low impeller speeds and constant projected pin surface area, whereas power draw varied more significantly as more pins were added. Therefore, the metric decreases. The simulations for constant projected area, were in agreement with these general trends, with the exception that at rotational speeds of below 150 rpm the 4-pin design exhibited a non-linear trend, showing increasingly poorer effectiveness as the impeller rotated more slowly. Overall the plot implies that although a higher pin count corresponds to more effective grinding due to greater force transfer to particles, as displayed in Fig. 9, the efficiency of force transfer generally

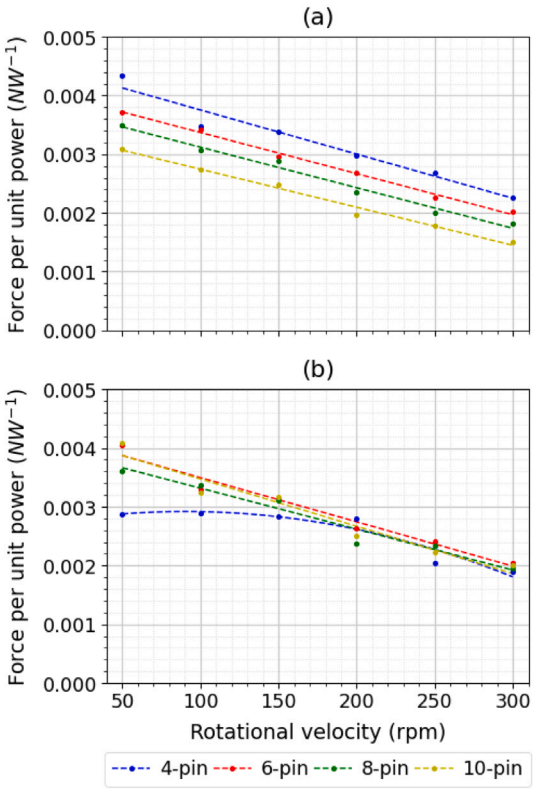

Fig. 13. Force transferred per unit of power dissipated for varying impeller rotational speed for systems of (a) constant pin size and (b) constant total pin projected surface area.

decreases because power dissipation becomes progressively larger as more pins are added.

Subsequently, the rotational speed of the media relative to the impeller was considered as this represented the impeller's capability of transferring kinetic energy amongst the beads. This is shown in Fig. 14. Similar to Fig. 13, the efficiency of the energy transfer shows a linear decrease as the impeller rotational speed increases. However, additional pins on the impeller shaft appear to generally improve the corresponding ratio. This result suggests that media are being more collectively propelled around the chamber as additional pins are included, potentially caused by smaller gaps between pins and a more even coverage of surface area, resulting in collective motion due to 'bridging'. The separation between pins becomes progressively smaller for higher pin designs, reducing from 38 mm in the 4-pin set up to 14 mm in the 10-pin set up (see Appendix A.1).

The 4-pin, constant area model showed unusual behaviour in both assessments of efficiency, with little force transfer per unit of power dissipated at low impeller speeds while showing relatively similar rotational motion between media and impeller. As a large portion of media occupy the lower region of the system when the impeller rotates slowly, the pins have a relatively large amount of contact with the media as the surface area of pins was located in the lower portion of the mill. Therefore, there was a large surface creating resistance to motion. However, because rotational speed is low, the force transfer is little and turbulence is less prevalent; the latter contributing further to the lack of force transfer. Comparing the granular temperature at impeller speeds of 50 rpm and 300 rpm shows there is a huge difference in the uniformity of motion, with the lowest rotational speed producing an average granular temperature of $0.0021\,m^2\,s^{-2}$, around $1/25$ in comparison to the granular temperature obtained at the highest rotational speed which was approximately $0.052\,m^2\,s^{-2}$. Thus, it justifies the lack of turbulence for the 4-pin design, and consequent rigid body-like motion, when rotating at slow speeds.

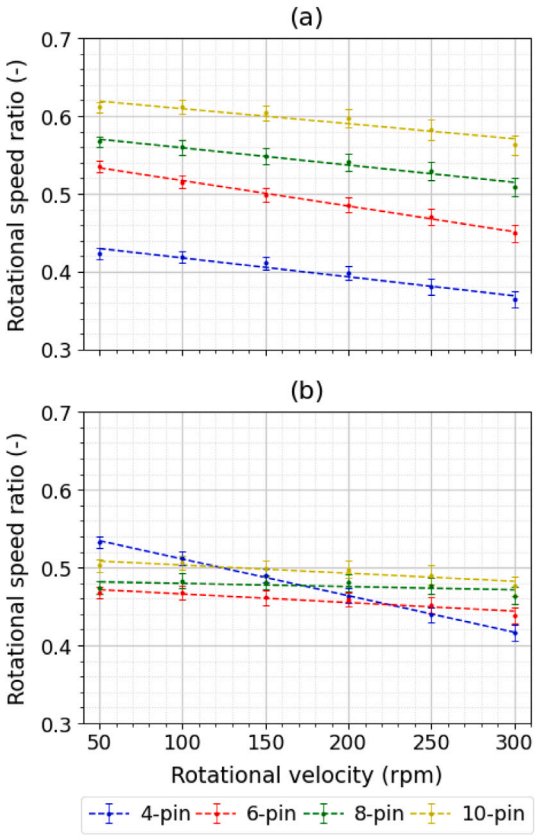

Fig. 14. Ratio of average particle rotational speed and the rotational speed of the impeller for systems of (a) constant pin size and (b) constant total pin projected surface area.

4. Validity

4.1. Media restitution

While most industrial mills operate under wet conditions, the study has only used a granular solving method in DEM. The fluid has been assumed as the media restitution value of 0.7, with any lubrication between the media on impact softening the collision.

To test the validity of this, the simulations were re-run using restitution values of 0.1, 0.3 and 0.5. The power draw for the constant pin size simulations are presented in Fig. 15. As one may intuitively expect, media possessing lower restitution coefficients induce greater power draw, with the effect being most pronounced at higher rpm as a greater propensity of contact events can be expected. Nonetheless, despite the quantitative differences observed for different restitutions, the qualitative trends as pin number is varied remains consistent across the full range of values explored. The same general trends can also be made for the constant total area simulations shown in Fig. 16.

Fig. 17 shows that there is an increase in the net force on each media as restitution increases. This is expected because the impacts from the contacts are expected to store more of the momentum at higher restitution values. Once again, the trends observed are the same, both in terms of linearity with rotational velocity and the values observed for each design with respects to the others. Because no grinding has occurred within the simulations, the study is only able to return an approximation of the grinding possible within the milling environment. However, these results demonstrate that our key conclusions are independent of the media properties.

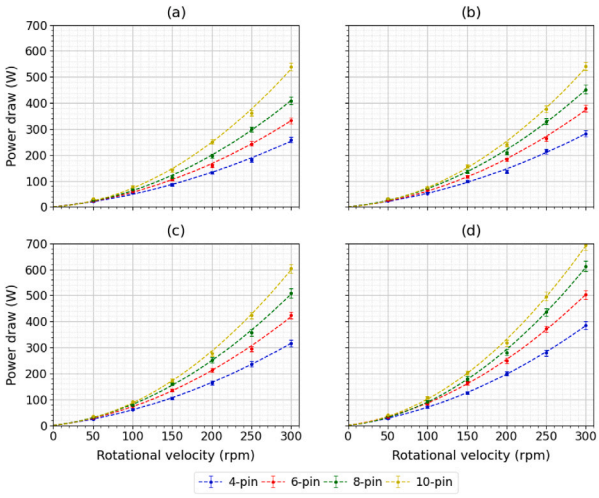

Fig. 15. Power draw from the constant pin size setup at different media restitution values. (a) 0.7 (original value), (b) 0.5, (c) 0.3 and (d) 0.1.

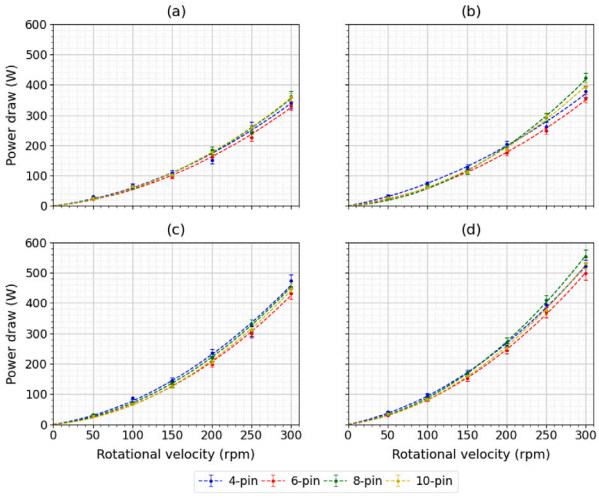

Fig. 16. Power draw from the constant total area setup at different media restitution values. (a) 0.7 (original value), (b) 0.5, (c) 0.3 and (d) 0.1.

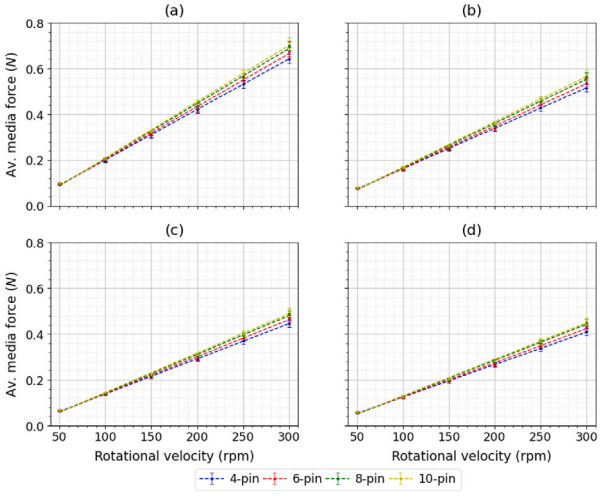

Fig. 17. Average net media force from the constant total area setup at different media restitution values. (a) 0.7 (original value), (b) 0.5, (c) 0.3 and (d) 0.1.

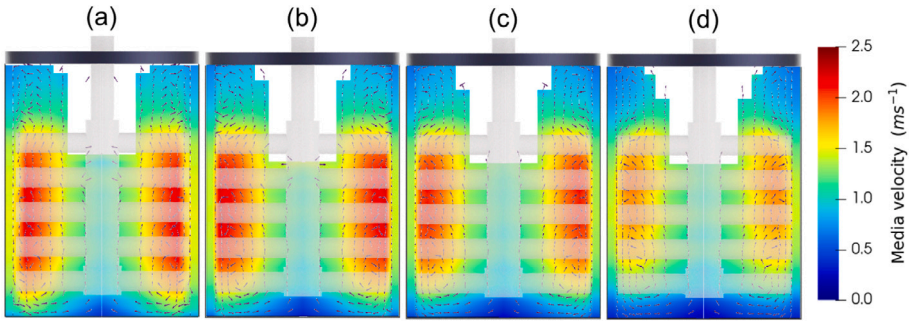

Fig. 18. Velocity fields using different media sizes at 300 rpm with the 10-pin equal pin size design. (a) 10 mm (original value), (b) 8 mm, (c) 6 mm, (d) 4 mm.

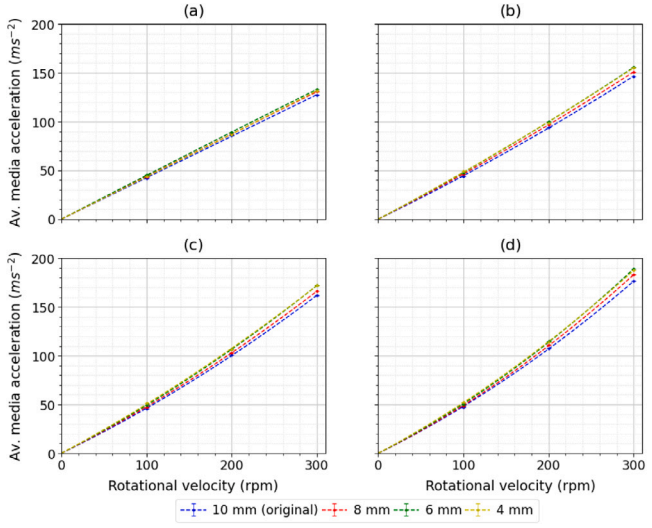

Fig. 19. Average media acceleration different rotation speeds, normalised with respect to media size for different configurations in the equal pin size study. (a) 4-pin, (b) 6-pin, (c) 8-pin, (d) 10-pin.

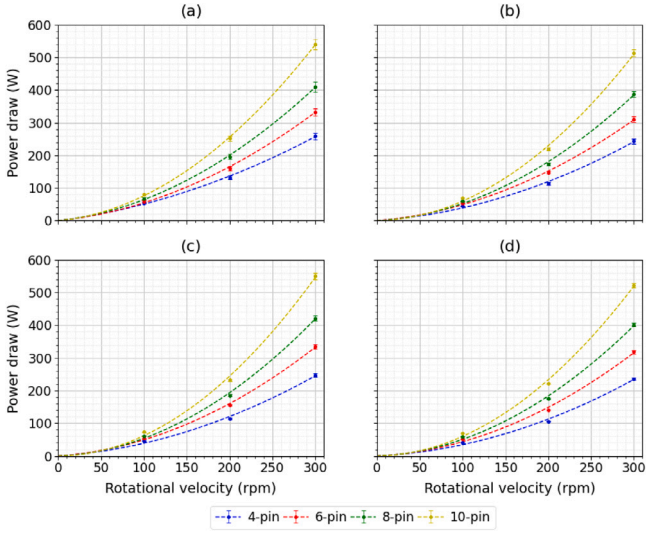

Fig. 20. Average power draw at different rotation speeds, media sizes and configurations in the equal pin size study. (a) 10 mm, (b) 8 mm, (c) 6 mm, (d) 4 mm.

4.2. Media size

One of the other media properties which will have an effect on the milling dynamics is the bead size. This creates an interaction effect between the geometry and media. If the velocity fields for the 10-pin constant pin design, at 300 rpm are displayed with media diameters of 10 mm (Fig. 18(a)), 8 mm (b), 6 mm (c) and 4 mm (d), there is a difference in average media velocity between the 4 mm bead and the rest. Each simulation has the same volume of media, and the overall flow patterns are very similar but the magnitude is lower because the smaller beads can get between adjacent flights more easily. There is also a larger dead zone at the bottom because more layers of media can fit under the bottom pair of pins. Despite small differences in the velocity fields, the media acceleration is comparable to within 10% across all sizes (Fig. 19). Acceleration has been used, as opposed to force, because it normalises the different media sizes by mass ($F = ma$). This means the media force exerted is directly proportional to the mass of the individual media and is significant because it can be used to predict contact forces. It also applies across all designs tested which means it is independent of the specific configuration used.

Finally, the power for each simulation, Fig. 20, shows that the qualitative and quantitative nature of changing the media size is largely insignificant. This is to be expected due to conservation of energy laws, as the same amount of input energy is provided by each attritor, but are significant because the individual contact energies will change with respect to size. Larger media carry greater momentum but there will be fewer contact events between them. If the combined dissipation of all contacts is similar, an engineer can therefore make decisions of whether the number of contacts or the individual magnitudes are more important within the mill design.

4.3. Variation with scaling

Ultimately, the results observed should have the ability to be scaled, as most industrial systems operate on much larger chamber volumes. Therefore, each design was run at 150 rpm using the same media and percentage fill level, but with double-size geometry. 150 rpm was used as it meant the tip speed was equivalent of 300 rpm at the original size, so the results could be compared by both that and the rpm.

Fig. 21 shows the power draw obtained by the constant area simulations with the equivalent rotational speed (150 rpm), and equivalent tip speed (1.30 m s^{-1}, 300 rpm) or the original geometry, scaled according to the predictions made by Radziszewski [11,40] (Eq. (9)) for comparison. These show differences, with the double scale geometry falling between the equivalent attritor rotational and tip speed. The general trend fits more closely with equivalent rpm, which is to be expected as those are the same units as the design equation. The reason for this is that the gap between the pin tip and chamber wall is only 12 mm in the original design; only just greater than the media diameter of 10 mm. Doubling this space, while keeping the media size the same, allows for more media to be consistently within this gap, and provide a more consistent reading. This will in turn affect the perceived viscosity of the system, and hence, the slightly lower scaled power for the larger geometry.

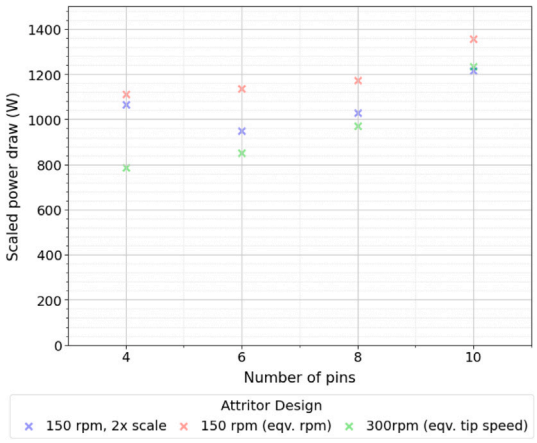

Fig. 21. Scaled power draw of the 10-pin constant area model under three conditions. (Blue) Double scaled geometry at 150 rpm, (Red) Original size geometry at the equivalent rpm of the larger model, (Green) Original size geometry at the equivalent tip speed of the larger model.

5. Conclusion

The study explored the grinding media dynamics of different vertical attritor mills. The biggest impact to changing conditions is by increasing the projected area that the pins are able to deliver to the beads as there is a greater area for surface transfer between attritor and media. However, the configuration also has an effect, leading to a proposal that the power draw equation by Radziszewski needs to include the shear volume between pins as part of the summation. Different options are more suitable depending on if the grinding happens at low or high velocity. Fewer, fatter pins are better for low velocity grinding while more pins offer greater energy transfer at higher speeds. This is important depending on the application, with some industries, such as food, dealing with soft particles that break down at much lower energies so do not need the speeds observed in other industries like mineral ore processing.

While the study is limited to only providing a probability of grinding, the results are industrially relevant as they provide a strong set of guidelines for system designers, and these are independent of media properties. Though providing lower force transfer, fewer pins will transfer energy more efficiently, potentially leading to design with fewer fatter pins that are not only energy saving but also more durable. With energy and climate being an increasingly large topic of conversation, these guides could lead to important savings across the industry.

CRediT authorship contribution statement

T. Osborne: Methodology, Investigation, Formal analysis, Writing – original draft. **D. Rhymer:** Formal analysis, Data curation, Writing – review & editing, Supervision. **D. Werner:** Software, Formal analysis. **A. Ingram:** Supervision, Writing – review & editing. **C.R.K. Windows-Yule:** Supervision, Writing – review & editing.

Declaration of competing interest

The authors declare the following financial interests/personal relationships which may be considered as potential competing interests: Daniel Rhymer reports financial support was provided by Engineering and Physical Sciences Research Council.

Data availability

Data will be made available on request.

Acknowledgements

The corresponding author is studying for an Engineering Doctorate (EngD) at the University of Birmingham, and acknowledges funding received from the Centre for Doctoral Training in Formulation Engineering, UK via the Engineering and Physical Sciences Research Council and Mondelēz International. (EPSRC Grant no. EP/S023070/1).

Nomenclature

Symbol	Definition	Units
A	Shear area	m^2
D	Pin diameter	mm
d	Media diameter	mm
E	Collision energy	J
E^*	Effective Young's modulus	Pa
F_{ij}	Contact force	N
G^*	Effective shear modulus	Pa
g	Gravitational acceleration	$m\ s^{-2}$
I	Moment of inertia	$kg\ m^2$
K	Stiffness	$N\ m^{-1}$
m	Media mass	kg
n	Media number	–
P	Power	W
$\bar{R}^2$	Variance proportion	–
R	Particle radius	m
r_s	Shear radius	m
SI_M	Media stress intensity	$kg\ m\ s^{-1}$
t	Timestep	s
V_G	Granular temperature	$m^2\ s^{-2}$
v_{ij}^n	Relative normal velocity	$m\ s^{-1}$
v_{ij}^t	Relative tangential velocity	$m\ s^{-1}$
V_τ	Shear volume	m^3
y	Shear separation	m
γ	Damping coefficient	$N\ s\ m^{-1}$
δ_{ij}	Media overlap	m
ϵ	Coefficient of restitution	–
η	Dynamic viscosity	Pas
μ_r	Rolling friction coefficient	–
μ_s	Sliding friction coefficient	–
ν	Poisson ratio	–
ρ	Particle density	$kg\ m^{-3}$
τ_{ij}^t	Rolling friction coefficient	–
ω	Rotational velocity	$rads^{-1}$

Appendix. Location of pins and pin separation for each design

A.1. Constant pin size study

See Table A.1.

A.2. Constant projected area study

See Table A.2.

Table A.1
Geometrical parameters for the first experiment. The values for pin location are relative to the bottom of the impeller shaft.

# Pins	Pair	Height (mm)	z-Sep (mm)	V_τ (m^3)
10	1	13.6	14	0.0021
	2	47.6		
	3	81.6		
	4	115.6		
	5	149.6		
8	1	13.6	22	0.0017
	2	55.6		
	3	97.6		
	4	139.6		
6	1	13.6	30	0.0014
	2	63.6		
	3	113.6		
4	1	13.6	38	0.0010
	2	71.6		

Table A.2
Geometrical parameters for the second experiment. The values for pin location are relative to the bottom of the impeller shaft.

# Pins	D (mm)	Pair	Height (mm)	z-Sep (mm)	V_τ (m^3)
10	12	1	15.0	20	0.0009
		2	47.0		
		3	79.0		
		4	111.0		
		5	143.0		
8	15	1	15.0	28	0.0011
		2	58.0		
		3	101.0		
		4	144.0		
6	20	1	15.0	36	0.0014
		2	71.0		
		3	127.0		
4	30	1	15.0	42	0.0021
		2	87.0		

References

[1] B. Blais, D. Vidal, F. Bertrand, G.S. Patience, J. Chaouki, Experimental methods in chemical engineering: discrete Element Method—DEM, Can. J. Chem. Eng. 97 (7) (2019) 1964–1973.

[2] T. Napier-Munn, Is progress in energy-efficient comminution doomed? Miner. Eng. 73 (2015) 1–6.

[3] J. Bouchard, A. Desbiens, E. Poulin, Reducing the energy footprint of grinding circuits: the process control paradigm, IFAC-PapersOnLine 50 (1) (2017) 1163–1168.

[4] A. Jankovic, Variables affecting the fine grinding of minerals using stirred mills, Miner. Eng. 16 (4) (2003) 337–345, http://dx.doi.org/10.1016/S0892-6875(03)00007-4.

[5] A. Jankovic, A review of regrinding and fine grinding technology-the facts and myths, in: Metso Miner Process Technol Asia-Pac, 2008.

[6] A. Kwade, Wet comminution in Stirred Media Mills—research and its practical application, Powder Technol. 105 (1–3) (1999) 14–20.

[7] Union Process, Dry batch or continuous LABORATORY MILLS, 2021, [Online] Available: https://www.unionprocess.com/attrition-mills/dry-attrition-mills/dry-grinding-laboratory-mills/dry-batch-or-continuous-laboratory-mills, [30/08/2021].

[8] M. Sinnott, P.W. Cleary, R. Morrison, Analysis of stirred mill performance using DEM simulation: Part 1–Media motion, energy consumption and collisional environment, Miner. Eng. 19 (15) (2006) 1537–1550.

[9] H.-H. Stender, A. Kwade, J. Schwedes, Stress energy distribution in different Stirred Media Mill geometries, Int. J. Miner. Process. 74 (2004) S103–S117.

[10] S. Breitung-Faes, A. Kwade, Use of an enhanced stress model for the optimization of wet Stirred Media Milling processes, Chem. Eng. Technol. 37 (5) (2014) 819–826.

[11] P. Radziszewski, Assessing the Stirred Mill design space, Miner. Eng. 41 (2013) 9–16.

[12] C. Tokoro, Y. Ishii, Y. Tsunazawa, X. Jiang, K. Okuyama, M. Iwamoto, Y. Sekine, Optimum design of agitator geometry for a dry Stirred Media Mill by the Discrete Element Method, Adv. Powder Technol. 32 (3) (2021) 850–859.

[13] V. Monov, B. Sokolov, S. Stoenchev, Grinding in ball mills: modeling and process control, Cybern. Inf. Technol. 12 (2) (2012) 51–68.

[14] D. Daraio, J. Villoria, A. Ingram, A. Alexiadis, E. Stitt, M. Marigo, Investigating grinding media dynamics inside a Vertical Stirred Mill using the Discrete Element Method: effect of impeller arm length, Powder Technol. 364 (2020) 1049–1061.

[15] D. Rhymer, A. Ingram, K. Sadler, C. Windows-Yule, A discrete element method investigation within vertical stirred milling: changing the grinding media restitution and sliding friction coefficients, Powder Technol. 410 (2022) 117825, http://dx.doi.org/10.1016/j.powtec.2022.117825.

[16] C. Zheng, L. Zhang, N. Govender, C.-Y. Wu, DEM analysis of residence time distribution during twin screw granulation, Powder Technol. 377 (2021) 924–938.

[17] C. Moliner, F. Marchelli, B. Bosio, E. Arato, Modelling of spouted and spout-fluid beds: key for their successful scale up, Energies 10 (11) (2017) 1729.

[18] A. Anand, J.S. Curtis, C.R. Wassgren, B.C. Hancock, W.R. Ketterhagen, Predicting discharge dynamics from a rectangular hopper using the Discrete Element Method (DEM), Chem. Eng. Sci. 63 (24) (2008) 5821–5830.

[19] E. Alizadeh, F. Bertrand, J. Chaouki, Comparison of DEM results and Lagrangian experimental data for the flow and mixing of granules in a rotating drum, AIChE J. 60 (1) (2014) 60–75.

[20] C. Coetzee, Calibration of the discrete element method, Powder Technol. 310 (2017) 104–142.

[21] C. Windows-Yule, A. Neveu, Calibration of DEM simulations for dynamic particulate systems, Pap. Phys. 14 (2022) 140010.

[22] J.K. Jiang, W.M. Dong, Z. Su, Study of stirrer disc structure type on grinding performance of a horizontal stirred mill, Appl. Mech. Mater. 779 (1) (2015) 156–159.

[23] D. Stief, W. Lawruk, L. Wilson, Tower mill and its application to fine grinding, Min. Metall. Explor. 4 (1) (1987) 45–50.

[24] T. Plochberger, M.B. Avila, Development of an energy optimized Stirred Media Grinding Mill, BHM Berg-und Hüttenmännische Monatshefte 159 (6) (2014) 253–258.

[25] P.W. Cleary, M. Sinnott, R. Morrison, Analysis of Stirred Mill performance using DEM simulation: part 2–coherent flow structures, liner stress and wear, mixing and transport, Miner. Eng. 19 (15) (2006) 1551–1572.

[26] C. Eswaraiah, N. Venkat, B. Mishra, R. Holmes, A comparative study on a vertical stirred mill agitator design for fine grinding, Sep. Sci. Technol. 50 (17) (2015) 2639–2648, http://dx.doi.org/10.1080/01496395.2015.1065888.

[27] CFDEMresearch, LIGGGHTS open source discrete element method particle simulation code, 2011, [Online] Available: https://www.cfdem.com/liggghts-open-source-discrete-element-method-particle-simulation-code, [23/05/2021].

[28] D. Zhao, E.G. Nezami, Y.M. Hashash, J. Ghaboussi, Three-dimensional discrete element simulation for granular materials, Eng. Comput. (2006).

[29] S.B. Yeom, E.-S. Ha, M.-S. Kim, S.H. Jeong, S.-J. Hwang, D.H. Choi, Application of the discrete element method for manufacturing process simulation in the pharmaceutical industry, Pharmaceutics 11 (8) (2019) 414.

[30] D. Daraio, J. Villoria, A. Ingram, A. Alexiadis, E. Hugh Stitt, M. Marigo, Validation of a discrete element method (DEM) model of the grinding media dynamics within an attritor mill using positron emission particle tracking (PEPT) measurements, Appl. Sci. 9 (22) (2019) http://dx.doi.org/10.3390/app9224816.

[31] K.C. Radil, A.B. Palazzolo, Influence of Temperature and Impact Velocity on the Coefficient of Restitution, National Aeronautics and Space Administration, 1994.

[32] K. Windows-Yule, L. Nicuşan, M.T. Herald, S. Manger, D. Parker, Comparison with other techniques, in: Positron Emission Particle Tracking, 2053-2563, IOP Publishing, 2022, http://dx.doi.org/10.1088/978-0-7503-3071-8ch4, 4–1 to 4–118.

[33] I. Goldhirsch, Introduction to granular temperature, Powder Technol. 182 (2) (2008) 130–136.

[34] S. Beinert, G. Fragnière, C. Schilde, A. Kwade, Analysis and modelling of bead contacts in wet-operating stirred media and planetary ball mills with CFD-DEM simulations, Chem. Eng. Sci. 134 (2015) (2015) 648–662, http://dx.doi.org/10.1016/j.ces.2015.05.063.

[35] C. Ndimande, P. Cleary, A. Mainza, M. Sinnott, Using two-way coupled DEM-SPH to model an industrial scale Stirred Media detritor, Miner. Eng. 137 (2019) 259–276.

[36] R. Roufail, B. Klein, Mineral liberation and particle breakage in Stirred Mills, Can. Metall. Q. 49 (4) (2010) 419–428.

[37] R. Hogg, Breakage mechanisms and mill performance in ultrafine grinding, Powder Technol. 105 (1–3) (1999) 135–140.

[38] J. Herbst, J. Sepulveda, Fundamentals of fine and ultrafine grinding in a Stirred Ball Mill, in: International Powder and Bulk Solids Handling Conference, Chicago, IL, Vol. 1, Elsevier, 1978, pp. 452–470.

[39] A. Kwade, L. Blecher, J. Schwedes, Motion and stress intensity of grinding beads in a Stirred Media Mill. Part 2: stress intensity and its effect on comminution, Powder Technol. 86 (1) (1996) 69–76.

[40] P. Radziszewski, J. Allen, Towards a better understanding of Stirred Milling technologies-estimating power consumption and energy use, in: 46th Annual Canadian Mineral Processors Operators Conference, Vol. 1, Elsevier, 2014, pp. 55–66.

[41] M.-W. Gao, K.S.E. Forssberg, K.R. Weller, Power predictions for a pilot scale stirred mill, Int. J. Miner. Process. 44–45 (1996) 641–652, http://dx.doi.org/10.1016/0301-7516(95)00072-0.

[42] B. Kumar, Energy dissipation and shear rate with geometry of baffled surface aerator, Chem. Eng. Res. Bull. 14 (2) (2010) 92–96.